Amylose chain behavior in an interacting context I. Influence of a nonchair ring on the maltose conformations

Gwenaëlle André-Leroux, Alain Buleon, Vinh Tran, F. Vallée, M. Juy, R. Haser

G. André
A. Buléon
V. Tran*
Laboratoire de Physico-Chimie des Macromolécules
INRA
BP 1627-44316
Nantes Cedex 03
France

F. Vallée
M. Juy
R. Haser
Laboratoire de Cristallisation et Cristallographie des Macromolécules Biologiques
IFRC1-CNRS 31
Chemin Joseph Aiguier 13402
Marseille Cedex 20
France

Amylose Chain Behavior in an Interacting Context I. Influence of a Nonchair Ring on the Maltose Conformations

*In the presence of steric constraints, flexible forms, i.e., skew (**S**), boat (**B**) or half-boat (**H**), were evoked from experimental data and conformational analyses by molecular mechanics calculations for glucopyranose rings of amylose fragments. This important case, occurring, for example, in amylose–amylase complexes, requires careful analysis of these flexible ring forms prior to any further conformational study. The influence of a nonchair (flexible) form on the maltose conformation is systematically evaluated, with an appropriate strategy using "semirelaxed" maps and comparing them with those obtained from already known chair–chair ($^4C_1$-$^4C_1$) maps. Therefore, new low-energy maltose conformations are described and classified from flexible-chair and chair-flexible maps. These conformations are well dispersed inside significantly larger contours in the (φ, ψ) projection. In a second stage, the consequence of these flexible ring forms is discussed in terms of amylose propagation apart from these new maltose conformations. Two propagation parameters are defined (τ, Ω), related to the local curvature of the chain and the relative orientation of the two mean ring planes. Low-energy conformations of $^4C_1$-$^4C_1$ maltose have almost the same curvature between the two rings, whereas their relative orientations have well-identified Ω values. On the contrary, the presence of one flexible conformation considerably increases the variation range of both propagation parameters. Thus, new low-energy conformations allow local curvatures yielding from almost perpendicular to linear pairs of glucopyranose rings with relative orientation covering about three-fourths of the total domain. This description is essential to understand amylose conformations in catalytic site and subsites of the amylases.* © *1996 John Wiley & Sons, Inc.*

Received July 20, 1995; accepted March 5, 1996
* To whom correspondence should be addressed.
Biopolymers, Vol. 39, 737–751 (1996)

CCC 0006-3525/96/050737-15

INTRODUCTION

Monosaccharides and oligosaccharides have been extensively studied as conformational precursors of biopolymers by means of computer modeling techniques. From detailed conformational studies of oligomeric fragments, 3-D representations of corresponding polysaccharides were derived for a better understanding of their physical and biological properties. Among the abundant literature, the paper by French and Brady[1] gives a general overview of this field in terms of strategies as well as theoretical and technical limitations. Within this framework, disaccharides are the smallest molecular entities necessary to generate regular or statistical linear homopolymers according to the glycosidic junction taken into consideration.[2-6]

The maltose molecule was widely studied in the past as a precursor of the amylose chain or cyclodextrins. This disaccharide is made up of two glucopyranose rings linked by a rather flexible α(1-4) glycosidic junction. Rigid[2,7-9] or flexible[10-12] monomer units were successively employed in molecular mechanics (MM) schemes depending on the expected accuracy of the calculations. As far as we know, all previous MM calculations on maltose assumed glucopyranose rings to adopt the most stable chair conformation ($^4C_1$). This assumption is quite acceptable in the absence of external constraints, and it sounds reasonable to consider that the two six-membered rings fluctuate around this stable conformation, in vacuum as well as in aqueous solution, whatever the glycosidic junction conformation may be. This flexibility of the glucopyranose unit has been extensively analyzed[13] by different molecular mechanics force fields and is confirmed by a survey of crystallographic structures containing pyranose rings.[14]

However, submitted to specific constraints, the glucopyranose rings can adopt higher energy forms as observed in the crystal structure of the dimeric cyclic derivative of gentiobiose.[15] This compound has two $\alpha(1-6)$ glycosidic linkages, and the internal cyclization leads to a constrained disaccharide where glucopyranose rings adopt in the same crystal both skew (*S* also called twist) and boat (*B*) forms. Other constraints on glucose residues stem from external steric conflicts occurring in glycosilase–oligosaccharide complexes in either site of the enzyme (active as well as secondary ones). Glucoamylases and amylases provide several cases where distortions of the six-membered ring out of the most stable conformation have been suspected. In 1960, Thoma and Koshland[16] suggested that the action of the β-amylase on saccharidic substrates necessitates at least the conformational change of one glucose residue from chair (*C*) to boat (*B*) form in the active site.

Since the complex between the glycosilase and the corresponding substrate cannot be resolved experimentally, Truscheit et al.[17] suggested that inhibitors could model the transition-state analog of glucose residue in the catalytic site. This assumption, now widely admitted, is consistent with the deformation of some glucose residues. In the glucoamylase case, several complexes with inhibitors were crystallized and resolved. With acarbose,[18] the binding constant, close to 10^{12} M^{-1}, is the largest one ever reported between a protein and a carbohydrate.[19] With this pseudo-tetrasaccharide, the double bond in the nonreducing ring induces a flexible conformation[20] that could be adopted by the corresponding glucopyranose ring during the catalytic action. Furthermore, the glucose configuration isomer obtained by the hydrogenation of the double bond has a far lower binding constant[19] (about $3 \cdot 10^7$ M^{-1}) because of the chair form of this ring.[21] The structure of 1-deoxynojirimycin/glucoamylase complex resolved by Harris et al.[22] shows that the $^4C_1$ conformation of the six-membered ring inhibitor is more favorable than the half-chair (*H*) conformation. However, these authors also showed by molecular mechanics calculations that the substitution of α-D-glucose for 1-deoxynojirimycin in the active site may favor (*H*) conformation. Similarly, the α-amylase/inhibitor complexes[23-26] suggest the possibility of a distortion of glucose residues at specific regions of the catalytic site. In the pancreatic α-amylase case, the complex obtained when soaking with acarbose was crystallized and refined to 2.2 Å resolution.[27] The resulting pseudo-pentasaccharide ligand kept the cyclitol ring in a half-chair conformation. This distortion of the six-membered ring from the $^4C_1$ conformation led to the interresidue torsion angles for the pseudo-disaccharide acarviosine ($\varphi\{C_7 - C_1 - N_1 - C_4\} = 18°$; $\psi\{C_1 - N_1 - C_4 - C_5\} = 149°$) that do not correspond to low energy conformations obtained from any published *C-C* adiabatic map. In a subsequent work[28] performed from these x-ray data, the molecular modeling refinement confirmed that (φ, ψ) values of acarviosine cannot correspond to known torsion angles between two $^4C_1$ sugar rings. Furthermore, the docking of the corresponding maltopentaose revealed that the glucopyranose ring replacing the cyclitol residue kept the most important ring deformation. In the Barley α-amylase case, the complex formed with

acarbose was also crystallized and refined to 2.8 Å.[29] Similarly, the cyclitol ring of the ligand adopts a half-chair conformation and the interresidue torsion angles of the acarviosine moiety cannot be satisfactorily superimposed on any ***C-C*** maps. Therefore, if one assumes that the geometries of the α-amylase inhibitors represent more or less that of amylose fragments before the catalytic action, flexible six-membered ring forms could be the crucial point of the modeling of these fragments at least in the active site.

From crystal structure determinations, the subsequent modeling of the interaction between glycosilase binding sites and saccharide necessitates a preliminary study of the incidence of glucopyranose flexible forms on maltose low energy conformations. Another important goal of this paper is to characterize the propagation on both sides of this disaccharide moiety and the orientation changes between the two-ring mean planes to explain possible binding of glucopyranose rings on specific protein sites and to provide insights into catalytic mechanism.

NOMENCLATURES AND CONVENTIONS

Several terminologies are mentioned in the literature to characterize the main six-membered ring conformations. This paper follows the nomenclature described by French and Brady (Fig. 3 of Ref. 1) which derives from that of Jeffrey and Yates.[30]

Cyclohexane Conformations

Because of the chemistry of carbon atoms (sp3 hybridization involving tetrahedral structure), the cyclohexane ring cannot be flat and must be puckered to respect the theoretical angle value of 109°47′. This induces different shapes among which the most known are chair (***C***) and boat (***B***) forms. The ***C*** forms, characterized by the alternation of endocyclic dihedral angle values of (+60°, −60°), have lower conformational energy than any alternative because all bonds are staggered and all axial hydrogen atoms cannot repel. Hazebroek and Oosterhoff[31] showed that ***B*** forms correspond to particular conformations among an infinity of solutions called "flexible" forms (as opposed to "rigid" ***C*** conformations), which are all linked by continuous variations of endocyclic dihedrals. A unique pseudo-rotation phase describes the evolution of cyclohexane flexible forms that are not energetically equivalent for steric reasons (i.e., eclipsed and staggered hydrogens on each carbon atom). The complete variation of the pseudo-rotation phase leads to the energetic curve schematically shown in Figure 1 and six boat (***B***) and six skew (***S*** also called twist) conformations alternatively occur. Table I gives some examples of typical dihedrals for ***C***, ***B***, and ***S*** forms. Compared with ***C*** forms, ***B*** ones are unlikely to be energetically favorable because of the eclipsed bonds, whereas ***S*** forms allow some staggered bonds. Thus, the energy values of ***S*** forms are intermediate between ***C*** and ***B*** forms.

Glucopyranose Conformations

With one oxygen atom in the skeleton, the corresponding six-membered pyranose ring belongs to the pyran class of molecules. The same sp3 hybridization of the oxygen atom induces a slight ring deformation with C—O bond distance of about 0.145 nm and modified C—C—O and C—O—C angles. This disruption of the initial cyclohexane symmetry results in segregations inside each class of pyranose forms. Thus, the $^4C_1$ is the lowest chair energy conformation, and six different ***B*** and ***S*** forms are also possible.

Sheldrick and Akrigg[14] showed from a survey of 161 published structures containing pyranose rings that, in the absence of strong external steric constrains, the pyranose ring adopts the $^4C_1$ conformation, the average endocyclic torsion angle values of which are reported in Table I. These average values are slightly shifted from +60° and −60°. Substitutions of an hydrogen atom of the carbons in axial or equatorial position by a primary or secondary hydroxyl group are possible and among the eight combinations of energetically favored substitutions, the glucopyranose configuration is one of the most stable due to four equatorial substitutions on C_2, C_3, C_4, and C_5 atoms. These substitutions enhance the differences between conformations belonging to the same class of forms (***C***, ***B***, or ***S***) in terms of energy and ring deformation. Moreover, ***B*** forms have especially unfavorable repulsions between groups attached to C_i and C_{i+3} carbon atoms compared with ***S*** forms that allow some bond staggering and relief of steric repulsions.

Puckering Parameters

From the pioneering work of Kilpatrick et al.[32] in 1947 on cyclopentane, Cremer and Pople[33] gave a general definition of the puckering of any monocyclic ring. The puckering parameters can be calculated from cartesian coordinates by analytical expressions. In the six-membered ring, three puckering parameters (Q, θ, Φ) are necessary to characterize ring conformations:

- Q: average deviation of atomic positions from the mean plane (in nm)
- θ: ($0 \leq \theta \leq \pi$) extent of distortion from the perfect $^4C_1$ conformation
- Φ: ($0 \leq \Phi \leq \pi$) phase angle (pseudo-rotation)

Figure 2 shows these three pucker parameters on half

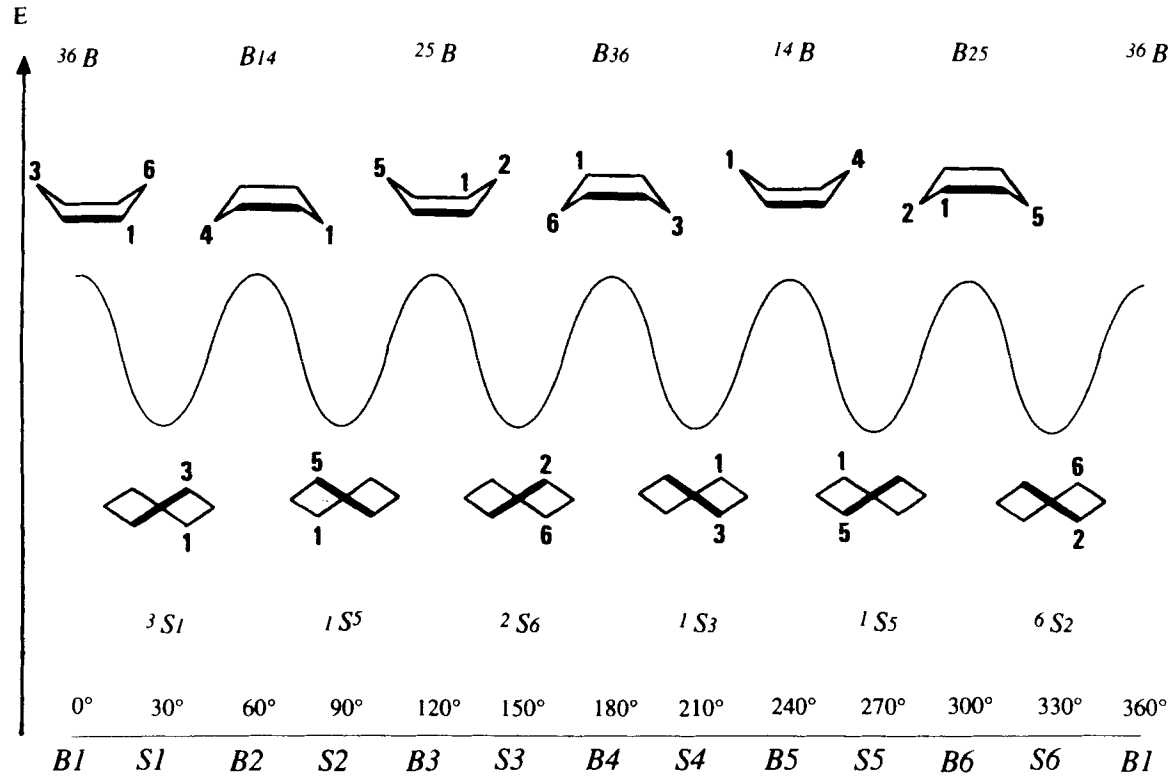

FIGURE 1 Schematic conformational energy fluctuations versus the pseudo-rotation phase Φ for flexible conformations of cyclohexane. The bottom labeling is used in this present work.

a sphere. In the cyclohexane case, the *C* conformation corresponds to (Q = 0.063 nm, θ = 0°, whereas the Φ parameter has no meaning) and is located on the pole. As an illustration of the pyranose case, the puckering parameters are calculated from the mean coordinates obtained by Sheldrick and Akrigg[14] (Q = 0.057 nm, θ = 2.02° and Φ = 340.5°). These values clearly show that $^4C_1$ average conformation is also located very near the

Table I Characterization of Six-Membered Ring Conformations

Conformation	$^4C_1$ Chair Cyclohexane	$^{1,4}B$ Boat Cyclohexane	S1 Skew Cyclohexane	$^4C_1$ Chair[a] Glucopyranose
Dihedral				
C_1–C_2–C_3–C_4	−60°	0°	26.96°	−53.51°
C_2–C_3–C_4–C_5	+60°	+60°	−54.76°	53.66°
C_3–C_4–C_5–C_6 or {C_3–C_4–C_5–O_5}	−60°	−60°	26.96°	−56.43°
C_4–C_5–C_6–C_1 or {C_4–C_5–O_5–C_1}	+60°	0°	26.96°	62.05°
C_5–C_6–C_1–C_2 or {C_5–O_5–C_1–C_2}	−60°	+60°	−54.76°	−62.21°
C_6–C_1–C_2–C_3 or {O_5–C_1–C_2–C_3}	+60°	−60°	26.96°	56.63°
Puckering parameter				
Q	0.63 Å	0.63 Å	0.63 Å	0.57 Å
θ	0°	90°	90°	2.0°
Φ	—	0°	30°	340.5°

[a] Average conformation according to Sheldrick and Akrigg.[14]

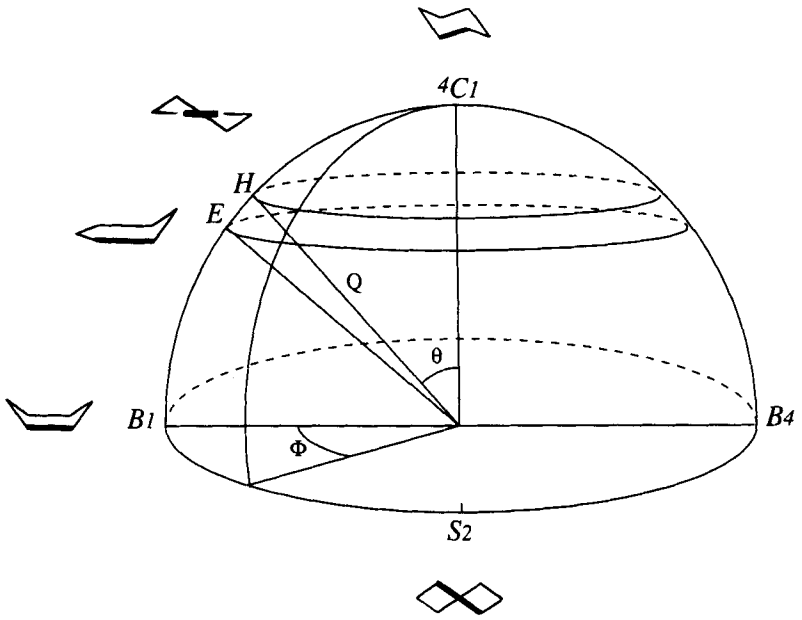

FIGURE 2 Representation of the spherical polar set of three puckering parameters and schematic view of the different kinds of rigid (***C***) and flexible (***B***, ***S***, ***E***, ***H***) six-membered ring conformations.

pole, and the only significant modification concerns the Q value, which is slightly lower.

Roundabout the equator of this sphere ($\theta = 90°$), as the phase angle Φ varies, the pseudo-rotational path traverses six boat conformations ***Bx*** (x = 1–6, according to the Φ values 0°, 60°, 120°, 180°, 240°, and 300°) and six skew conformations ***Sx*** (x = 1–6 with Φ = 30°, 90°, 150°, 210°, 270°, and 330°). Along the θ axis, other local minima energy forms are encountered and identified as envelopes (***E*** also called sofas or half-boats) and half-chairs (***H***), which correspond to (θ = 54.7°) and (θ = 50.9°), respectively (Figure 2). It must be mentioned that ***H*** forms often occur for rings with unsaturated carbon atoms.

Glycosidic Linkage

A schematic view of the maltose disaccharide is shown in Figure 3 along with the labeling of the atoms according to the convention used for saccharides. In this paper, the glycosidic dihedral angles are defined with nonhydrogen atoms as follows:

$$\varphi = \angle O_5\text{-}C_1\text{-}O_1\text{-}C'_4 \text{ and } \psi = \angle C_1\text{-}O_1\text{-}C'_4\text{-}C'_5$$

where the unprimed and primed residues refer to nonreducing and reducing ring, respectively. In addition to this, another convention is often used with hydrogen atoms:

$$\varphi^H = \angle H_1\text{-}C_1\text{-}O_1\text{-}C'_4 \text{ and } \psi^H = \angle C_1\text{-}O_1\text{-}C'_4\text{-}H'_4$$

Conversion between these two conventions is approximately:

$$\varphi \sim \varphi^H + 120°; \psi \sim \psi^H - 120°$$

Procedure

As discussed above, any flexible form of the pyranose ring is less stable than $^4C_1$ form, and these forms can only occur in the presence of external constraints. Therefore, the systematic analysis by MM calculations of these non-

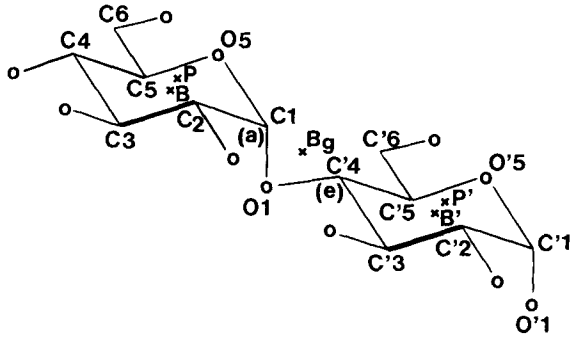

FIGURE 3 Schematic representation and labeling of the atoms of the maltose residue. *Bg*: barycenter of *C*1, *C*′4. *B*: barycenter of *C*1, *C*2, *C*3, *C*4, *C*5, and *O*5. *B*′: barycenter of *C*′1, *C*′2, *C*′3, *C*′4, *C*′5, and *O*′5. *P*: barycenter of *C*1, *O*5, *C*5, and *C*4. *P*′: barycenter of *C*′1, *O*′5, *C*′5, and *C*′4.

chair forms without these external constraints sounds a bit artificial. One must use mathematical conditions when exploring this higher energy space to avoid returning to the $^4C_1$ conformation during the minimization procedures. In addition to these constraints, "semirelaxed" strategy described below yields a conformational analysis less accurate than that using a fully "relaxed" one. Therefore, the simplest potential, consistent valence force field (CVFF),[34] available in the Discover package of BIOSYM company was chosen mainly to spare CPU time. This general force field, not being tailored for saccharides lacks, for instance, additional energy terms taken into account the exoanomeric effect, and it is obvious that it induces artifacts when applied to sugar molecules. Nevertheless, the resulting errors are negligible compared with the approximations assumed in this methodological approach. Thus, the CVFF potential was estimated fully appropriate for determining possible new regions in the (φ, ψ) space due to the ***S*** forms. Construction and visualization of molecules were done with the INSIGHTII package.

Initial Flexible Forms of Glucopyranose

Since the ***Sx*** forms are energetically favored compared with ***Bx*** ones, they were taken as reference for flexible forms because it is much easier to define local minima than metastable ***Bx*** forms (or even ***E*** and ***H*** ones). From an initial α-D-glucose molecule with $^4C_1$ conformation, the C_1-O_5 bond was broken to impose values for the three adjacent torsional angles $C_1-C_2-C_3-C_4$, $C_2-C_3-C_4-C_5$, $C_3-C_4-C_5-O_5$ on this open geometry. An appropriate combination of dihedral values corresponding to the cyclohexane in ***Sx*** forms ($\pm$54.76°, $\pm$26.96°) was initially imposed then, the C_1-C_5 bond was recreated to obtain the ring back. Since these values are not exactly those corresponding to low-energy conformations, small steric conflicts were suppressed by a relaxation of all internal parameters during a preliminary minimization stage that roughly kept the initial ***Sx*** geometries according to the third puckering parameter Φ.

Initial Maltose Constructions

Starting from these ***Sx*** conformations, 12 initial conformations were built, assuming that only 1 glucopyranose ring adopts a flexible form. Assuming that both rings could adopt flexible forms would mean considering a total of 36 initial geometries, considerably increasing the amount of calculations. Having in mind that these maps will be further used to analyze the propagation of amylose chain apart from this dimeric fragment in comparison with experimentally observed cases, it was decided that any peculiar ***Sx-Sy*** maltose map (with x, y = 1–6) will be drawn if such a case is encountered.

Therefore, two series of maltose maps (***Sx-C*** and ***C-Sx***) were considered depending on the presence of a flexible form on the reducing or nonreducing end. In the terminology adopted here, the geometry of the nonreducing ring is stated first and that of reducing ring second. ***Sx*** refers to one of the skew form and ***C*** to $^4C_1$ conformation. The initial geometries were built by branching a $^4C_1$ ring conformation on the desired flexible forms. For all molecules, oxymethyl groups were added to C_4 and C'_1 atoms to avoid spurious intraring hydrogen bond and to mimic the further propagation of the amylose chain at these ends. From these 12 starting geometries, some new minimizations were performed while only fixing the cartesian coordinates of the nonhydrogen atoms of the flexible form to relax the constraints mainly located around the glycosidic junction.

Semirelaxed Maltose Maps

The protocol was based on three successive stages. From the initial geometry, a preliminary rigid map was first performed on a (φ, ψ) grid (intervals of 5°) of parameters. For each (φ, ψ) set of values, the energy was calculated without any minimization and iso-energy contours were drawn to roughly determine the main local minima. In the second stage, from each identified local minimum, a complete minimization (steepest descent, 100,000 iterations) was carried out without any constraint on internal parameters of the molecule for a more accurate location of this minimum in the (φ, ψ) space. In practice, several combinations of primary and secondary hydroxyl groups orientations were manually tested. This nonautomatic procedure selected the best hydroxyl group orientations, and the lowest energy conformation obtained was kept as representative of this minimum. Nevertheless, according to the (θ, Φ) puckering parameters, the calculations that did not keep the initial ***Sx*** conformation for the flexible ring were discarded. For the θ parameter, the allowed variation was ($45° \geq \theta \geq 135°$) delimiting the distortion of ***S*** or ***B*** forms in direction of stable ***C*** conformation by approximately ***H*** forms. For the Φ phase, the allowed range was ($\Phi_0 - 30° \geq \Phi_0 \geq \Phi_0 + 30°$ with Φ_0 = 30°, 90°, 150°, 210°, 270°, and 330°). Thus each ***Sx*** conformation was delimited by the two adjacent ***B*** forms along the pseudo-rotation path. Finally, a third exclusion criterion based on the (φ, ψ) space was used when one local minimum converged toward another minimum region. In this case, the initial conformation was considered unstable and discarded for subsequent calculations. Assuming that each refined minimum conformation is representative of the surrounding region, all partial rigid maps based on local minimum conformations were then performed in the third stage. Finally, for a given map, all the partial rigid maps were merged in a global map (called semirelaxed map) by selecting for each (φ, ψ) set the lowest energy conformation.

Compared with a fully relaxed map (or adiabatic map), the basic difference in this semirelaxed procedure is that the relaxation of all internal parameters only occurs on specific geometries considered as representative

of the global or local minima regions. This "short-cut" procedure allows an enormous saving of time for a very acceptable accuracy as long as the location of all minima of interest has been correctly identified. The semirelaxed map of maltose with the two glucopyranose rings in $^4C_1$ chair conformation (*C-C* map) was also performed. This was mainly to allow comparisons between this strategy and fully relaxed ones already published,[10-12] although the used force fields were different. More interestingly, the comparison between *C-C*, *C-Sx*, and *Sx-C* maps provides information on the consequence of one flexible ring form in terms of location of low-energy regions, conformational energies, as well as general shapes of these maps.

Propagation of the Glucopyranose Rings

The characterization of the propagation of a glucopyranose ring from the previous adjacent one requires several parameters. However, one can focus on two main degrees of freedom, which are the curvature between the two adjacent rings and the relative orientation between their mean planes. The first parameter evaluates, residue per residue, the propagation of the amylose chain inside or outside the catalytic site, and the second parameter can give explanations about possible docking of these rings on subsites. These two propagation parameters could have several definitions depending on the pseudo-atoms taken into account. Here, we have chosen general definitions that could be used for any kinds of six-membered rings and glycosidic junctions. The curvature is described by the angle (τ) between three pseudo-atoms called B, B', and B_g (Figure 3). The first two correspond to the barycenter of each six-membered ring, whereas the third is the barycenter between the nearest atom of each ring (C_1 and C'_4). This medium point of the angle was found more representative than the glycosidic oxygen atom for the hinge between the two rings. The τ angle (*B-Bg-B'*) takes into consideration some information about maltose conformations such as the inherent ring forms, the linkage types on C_1 and C'_4 and the internal parameters of the glycosidic junction. To measure the relative orientation between the two mean ring planes, two other pseudo-atoms are defined (P and P') as the barycenters of the same half of the rings (C_1, O_5, C_5, C_4, and C'_1, O'_5, C'_5, C'_4, respectively) and the dihedral angle Ω (*P-B-B'-P'*) provides this orientation (Figure 3).

RESULTS AND DISCUSSION

C-C map

Figure 4 presents C-C maltose map performed with the semirelaxed strategy. This projection on the (φ, ψ) space must be compared with previous fully relaxed maps published by Ha et al. with CHARMM[10] and Tran et al. with a modified MM2

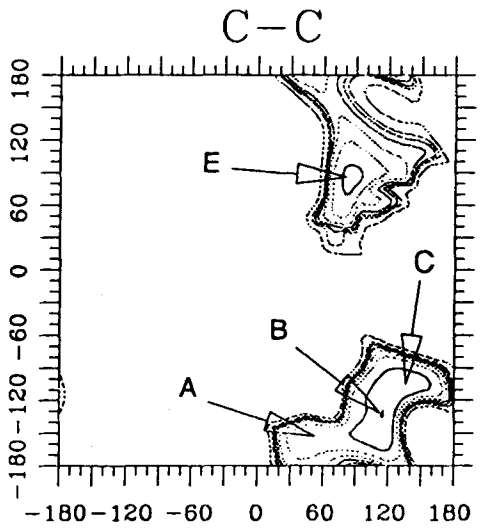

FIGURE 4 Semirelaxed *C-C* maltose map. Iso-energy contours are spaced at 5 kcal/mol intervals above the global minimum (*C-C*$_B$) until 30 kcal/mol. The outer contour corresponds to 50 kcal/mol above this minimum. (ϕ, ψ) Correspond to abscissa and ordinate, respectively.

force field.[11] For these two potentials specifically adapted for saccharides, a previous comparison[11] showed that the choice of a different force field has only a small influence upon the general shape of iso-energy contours as well as locations of minimum regions and relative energies between corresponding conformations. As mentioned above, the simplest force field (CVFF) associated to DISCOVER Package was used in the present case. Even if no specific terms for saccharides are present, it was previously successfully tested on amylose chain in another interacting context with fatty acids.[35] In such explicit or implicit interacting context (which is the case here), the external forces responsible for the maltose deformation are much more important than intrinsic energy terms that could be added due to specific saccharide effects. Therefore, the force field choice cannot explain the differences between the previous maps and that reported here. Indeed, the relaxation concept, which is known to considerably enhance the accessible (φ, ψ) regions, can account for some of the significant differences. The pure rigid approximation mainly takes into account the repulsive term of the Van der Waals, whereas the introduction of the internal flexibility (relaxation) decreases such a drastic effect by small displacements of atomic positions. Since the semirelaxed strategy used here (intermediate between rigid and relaxed ones) only permits a relaxation of the internal parameters of a

Table II Relative Energies and (ϕ, φ) Values of Probable Conformations Seen on *C-C* Semirelaxed Map

Zone	A	B	C	D	E	F	G
Energy (kcal/mol)	5.7	0.0	2.9		4.0		
ϕ (°)[a]	56	114	133		85		
	(60)	(120)	(140)	(70)	(90)	(70)	(140)
φ (°)[a]	−151	−133	−108		84		
	(−160)	(−130)	(−100)	(−80)	(80)	(50)	(100)

[a] Values in parentheses are the estimation of the low-energy zones of previous works.[10,11]

few identified conformations, the enhancement of the probable regions is less important than that observed in fully relaxed maps.

With the semirelaxed procedure, four low-energy conformations were found, three belonging to one continuous and rather compact zone ($30° > \varphi > 170°$, $-180° > \psi > -80°$) and the fourth one corresponding to an isolated zone ($60° > \varphi > 120°$, $40° > \psi > 120°$). For sake of consistency between the two previous relaxed maps,[10,11] the labeling of local minima was kept. The greater zone encompasses the *A*, *B*, *C* conformations in Ha's work, whereas an additional conformation (labeled *D*) was found in Tran's study. Here, the three main conformations (*A*, *B*, *C*) were identified inside this zone, only *B* being shifted. The smaller zone was less well isolated in the two previous works (due to the full relaxation procedure) with a common local minimum (*E*) also found in this work and two other minima (*G* and *F* for Ha's and Tran's work, respectively).

Finally, the comparison between the relaxed maps showed that the *A* or *B* conformations have the lowest energies. However, the segregation of these probable conformations (and of *C*) is less pronounced than in this present semirelaxed map. A more detailed analysis about the energy values could be hazardous due to the different force fields and strategies. For further energy comparisons between all minimum conformations obtained by this semirelaxed procedure, the lowest energy ever found (corresponding to *B* conformation of ***C-C*** map) will be used to calculate the relative energies of all other minima. Table II gives (φ, ψ) values and relative energies of the four probable conformations of this map and the low energy conformations are reported on Figure 5 with circle symbols.

C-Sx Maps

Table III summarizes all important features of this series of maps in terms of energy, puckering parameters, and (φ, ψ) values. The average of the relative energies reported on this table is about 16 kcal/mol higher than that of the lowest ***C-C*** conformation. Thus, the presence of a flexible ring at the reducing end results in a significant increase of the conformational energy. However, this investigation showed that low-energy conformations belong to rather stable subspaces since in only very rare cases, the reducing ring has converged toward the ***C*** form during the minimization procedure. These cases were discarded, and all the flexible conformations participating to these maps were checked according to the θ puckering parameter with a maximum deviation ($\theta = 82.9°$) toward the stable ***C*** form observed for the ***C-S1***$_E$. According to the puckering parameter Φ whose deviations from the corresponding theoretical value were less than ±30°, the ***Sx*** differentiation was respected.

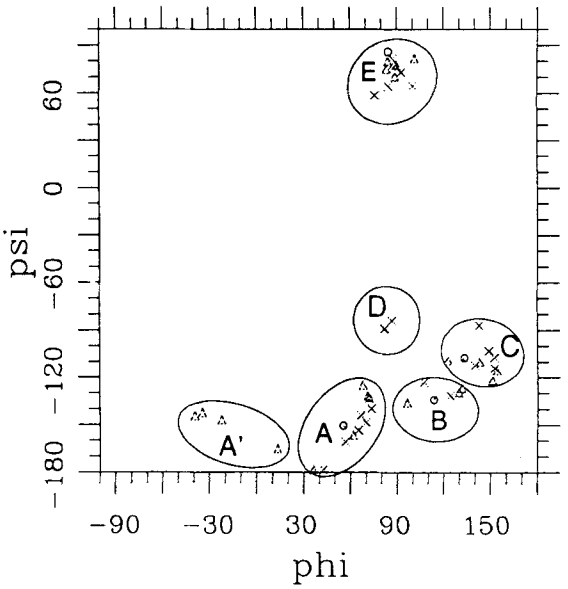

FIGURE 5 (ϕ, ψ) Location of low-energy conformations of all maps. Circle, cross, and triangle symbols refer to ***C-C***, ***C-Sx***, and ***Sx-C*** maps, respectively.

Table III Relative Energies and (ϕ, φ) values of Low-Energy Conformations Seen on *C-Sx* Semirelaxed Maps. The Reported Puckering Parameters Are Those of the Flexible Forms (Reducing Ring)

Type		A	B	C	D	E
C-S1	Energy (kcal/mol)	13.8		15.0	13.9	19.2
	ϕ(°)	70.5		142.6	87.0	84.9
	φ (°)	−148.6		−86.9	−83.9	64.1
	Pucker Q (Å)	0.69		0.69	0.69	0.62
	θ (°)	91.3		90.8	90.9	82.9
	Φ (°) theo. 30	16 (*S1*)		11 (*B1*)	17 (*S1*)	12 (*B1*)
C-S2	Energy (kcal/mol)	20.3		20.1	19.1	
	ϕ (°)	73.7		152.5	81.8	
	φ (°)	−139.8		−114.1	−89.2	
	Pucker Q (Å)	0.60		0.61	0.61	
	θ (°)	87.2		85.0	88.7	
	Φ (°) theo. 90	78 (*S2*)		85 (*S2*)	78 (*S2*)	
C-S3	Energy (kcal/mol)	17.0		15.7		20.6
	ϕ (°)	66.6		148.9		100.5
	φ (°)	−144.1		−102.9		64.5
	Pucker Q (Å)	0.63		0.63		0.62
	θ (°)	82.5		80.3		83.9
	Φ (°) theo. 150	152 (*S3*)		163 (*S3*)		139 (*S3*)
C-S4	Energy (kcal/mol)	14.3	11.9	12.1		13.1
	ϕ (°)	56.5	107.5	140.3		87.5
	φ (°)	−160.8	−123.0	−112.3		81.7
	Pucker Q (Å)	0.68	0.67	0.68		0.67
	θ (°)	85.3	85.4	84.2		87.5
	Φ (°) theo. 210	224 (*S4*)	213 (*S4*)	219 (*S4*)		223 (*S4*)
C-S5	Energy (kcal/mol)	12.0	9.3			16.8
	ϕ (°)	42.7	124.2			92.9
	φ (°)	−178.6	−131.4			72.8
	Pucker Q (Å)	0.66	0.66			0.65
	θ (°)	88.7	88.3			90.8
	Φ (°) theo. 270	272 (*S5*)	263 (*S5*)			258 (*S5*)
C-S6	Energy (kcal/mol)	16.0		18.8	14.9	18.3
	ϕ (°)	65.2		152.3	82.2	76.1
	φ (°)	−153.5		−107.2	−89.0	58.7
	Pucker Q (Å)	0.67		0.66	0.66	0.68
	θ (°)	91.6		92.1	90.5	88.2
	Φ (°) theo. 330	334 (*S6*)		345 (*S6*)	354 (*B1*)	321(*S6*)

However, in some cases (***C-S1***$_{C,E}$ and ***C-S6***$_D$), some adjacent ***B1*** forms were encountered.

For (φ, ψ), the previous labeling of the low-energy regions was kept for the five regions (*A*, *B*, *C*, *D*, and *E*). All low-energy conformations are plotted on Figure 5 with cross symbols and ***C-Sx*** maps are shown in Figure 6. The general shapes of all these maps must be examined according to a continuous variation of the Φ puckering parameter from ***C-S1*** to ***C-S6*** or conversely. The ***C-S4*** and, to a less extent, the adjacent ***C-S5*** map have iso-energy contours very similar to those of the ***C-C*** map because their corresponding low energy conformations are very close. The iso-energy contours of the other maps present a more extended accessible zone essentially due to the occurrence of the *D* region, clearly observed in ***C-S1*** and ***C-S6*** maps.

Sx-C Maps

As in the previous series of maps, Table IV summarizes all important features of low-energy conformations. The average of the relative energies is about 10 kcal/mol higher than that of the lowest ***C-C*** maltose conformation. This value is significantly lower than that calculated for the ***C-Sx*** maps, which means that the presence of a flexible form on the nonreducing ring creates steric perturbations

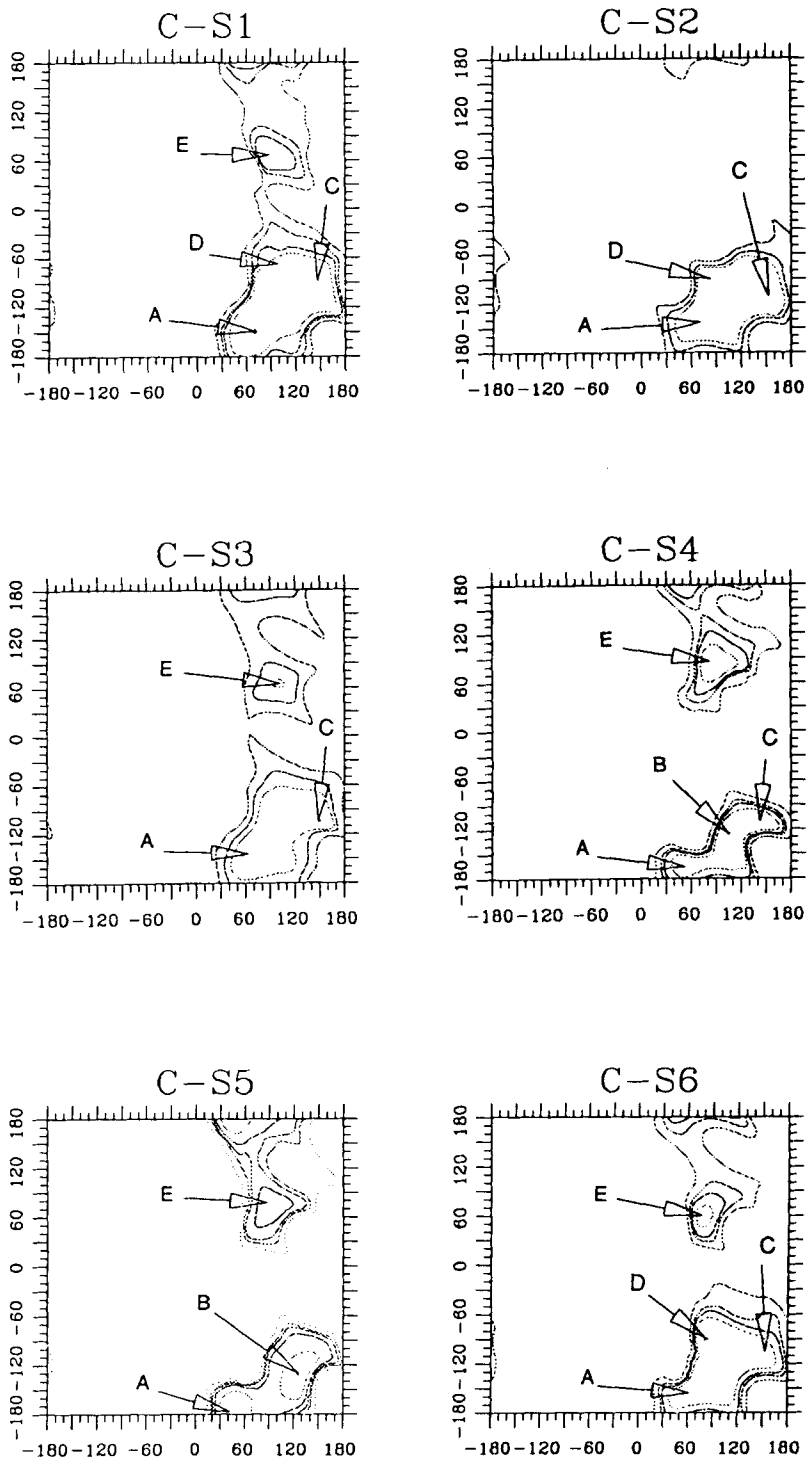

FIGURE 6 Semirelaxed *C-Sx* maltose maps. Relative iso-energy contours are spaced at 5 kcal/mol intervals above the absolute minimum (*C-C*$_B$) until 30 kcal/mol. The outer contour corresponds to 50 kcal/mol above this minimum. (ϕ, ψ) Correspond to absciss and ordinate, respectively.

globally better relaxed than in *C-Sx* cases. It must be mentioned that some conformations (*S1-C*$_B$ and *S4-C*$_A$) have low energies quite comparable with that of the most stable *C-C* conformation. As in the *C-Sx* series, *Sx-C* maps have stable subspaces where the flexible forms are well kept ac-

Table IV Relative Energies and (ϕ, φ) Values of Low-Energy Conformations Seen on *Sx-C* Semirelaxed Maps. The Reported Puckering Parameters Are Those of the Flexible Forms (Nonreducing Ring)

Type		A′	A	B	C	E
S1-C	Energy (kcal/mol)		7.3	6.6		11.3
	ϕ (°)		61.7	129.9		89.1
	φ (°)		−156.8	−129.4		70.2
	Pucker Q (Å)		0.67	0.68		0.69
	θ (°)		93.6	92.6		91.5
	Φ (°) theo. 30		9 (*B1*)	2 (*B1*)		3 (*B1*)
S2-C	Energy (kcal/mol)		13.3	11.3	15.7	17.0
	ϕ (°)		36.2	96.5	143.1	101.7
	φ (°)		−178.6	−136.0	−110.0	81.7
	Pucker Q (Å)		0.60	0.60	0.60	0.61
	θ (°)		87.3	87.3	83.7	83.9
	Φ (°) theo. 90		84 (*S2*)	85 (*S2*)	87 (*S2*)	84 (*S2*)
S3-C	Energy (kcal/mol)	11.4	8.8		10.2	12.3
	ϕ (°)	−22.0	72.3		122.7	83.7
	φ (°)	−147.0	−132.9		−109.2	74.9
	Pucker Q (Å)	0.60	0.62		0.61	0.64
	θ (°)	73.91	81.7		80.2	80.7
	Φ (°) theo. 150	51 (*S3*)	152 (*S3*)		141 (*S3*)	167 (*B4*)
S4-C	Energy (kcal/mol)	8.2	5.0		8.5	10.3
	ϕ (°)	−39.3	71.2		151.2	88.5
	φ (°)	−144.4	−131.7		−121.9	77.9
	Pucker Q (Å)	0.66	0.67		0.67	0.67
	θ (°)	85.1	86.1		86.8	87.4
	Φ (°) theo. 210	222 (*S4*)	220 (*S4*)		225 (*S4*)	222 (*S4*)
S5-C	Energy (kcal/mol)	8.3	8.5		8.2	10.9
	ϕ (°)	−34.2	68.1		154.1	84.4
	φ (°)	−142.3	−125.4		−115.6	79.9
	Pucker Q (Å)	0.66	0.67		0.65	0.67
	θ (°)	85.2	88.3		84.2	89.1
	Φ (°) theo. 270	274 (*S5*)	268 (*S5*)		269 (*S5*)	264 (*S5*)
S6-C	Energy (kcal/mol)	12.9		9.7		13.6
	ϕ (°)	13.3		131.5		90.0
	φ (°)	−165.3		−126.8		77.3
	Pucker Q (Å)	0.64		0.66		0.65
	θ (°)	97.2		93.5		94.0
	Φ (°) theo. 330	2 (*B1*)		357 (*B1*)		354 (*B1*)

cording to the θ puckering parameter. However, the number of observed ***B*** forms adjacent to initial ***S*** conformations is higher than in the ***C-Sx*** series (i.e., ***S1-C*** and ***S6-C***).

The six ***Sx-C*** maps are presented in figure 7. As to (φ, ψ) locations, the labeling of the low energy conformations used for ***C-Sx*** maps was kept for *A*, *B*, *C*, and *E* regions as reported on Figure 5 (with triangle symbols). None of the ***Sx-C*** maps revealed a *D* conformation but a new region, labeled *A′*, was found for some maps of this series. This region considerably increases the accessible (φ, ψ) space (essentially in φ dimension) and was never observed before, even in relaxed ***C-C*** maps. As before, the general shapes must be analyzed according to the continuous variation of the Φ puckering parameter (along the pseudo-rotation path). For the most extended zone (encompassing *A′*, *A*, *B*, and *C* regions), maps from ***S3-C*** and ***S6-C*** have typical iso-energy contours characterized by a very large φ domain due to the *A′* region. The two other maps ***S1-C*** and ***S2-C*** have general shapes rather similar to that of ***C-C*** map.

Propagation of the Glucopyranose Rings

To evaluate the influence of the ring forms on the propagation of the maltose molecule, the two pro-

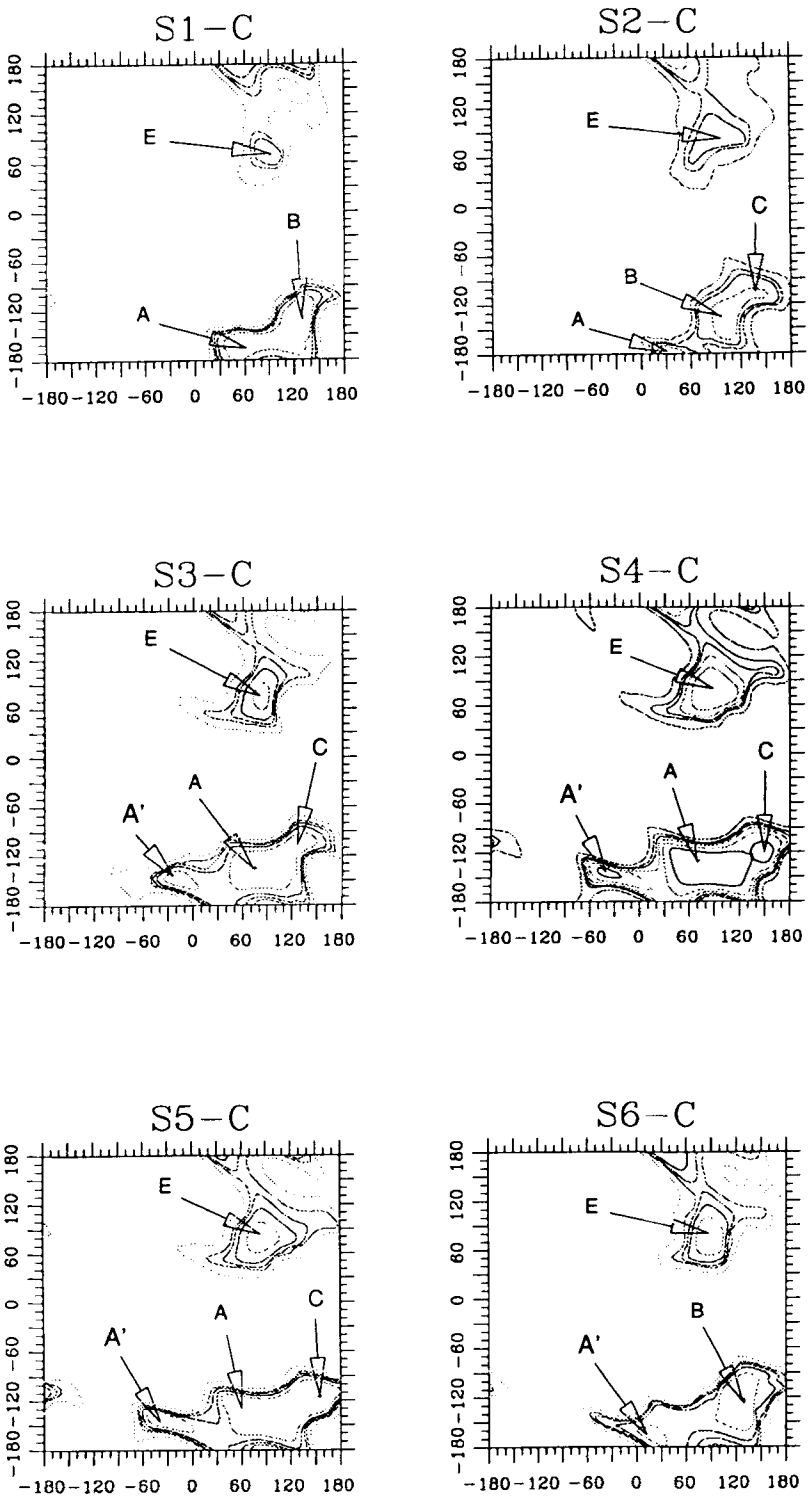

FIGURE 7 Semirelaxed ***Sx-C*** maltose maps. Relative iso-energy contours are spaced at 5 kcal/mol intervals above the absolute minimum (***C-C***$_B$) until 30 kcal/mol. The outer contour corresponds to 50 kcal/mol above this minimum. (ϕ, ψ) Correspond to absciss and ordinate, respectively.

pagation parameters (τ, Ω) were calculated for every low-energy conformations of ***C-Sx*** and ***Sx-C*** maps and then compared with those of ***C-C*** map.

Among the internal parameters responsible for the τ value, the linkage types on C_1 and C'_4 atoms were found predominant and are direct conse-

Table V Propagation Parameters (τ, Ω) Between the Two Glucopyranose Rings

Type	Linkage Type	τ (°)	Ω (°)	(ϕ, ψ)
(*C*-*C*)A	(*a* − *e*)	155	−80	(56; −151)
(*C*-*C*)B	(*a* − *e*)	155	−16	(114; −133)
(*C*-*C*)C	(*a* − *e*)	154	21	(133; −108)
(*C*-*C*)E	(*a* − *e*)	164	180	(85; 84)
(*C*-*S*1)A	(*a* − *a*)	143	−64	(71; −149)
(*C*-*S*1)C	(*a* − *a*)	138	52	(143; −87)
(*C*-*S*1)D	(*a* − *a*)	124	6	(87; −84)
(*C*-*S*1)E	(*a* − *a*)	147	165	(85; 64)
(*C*-*S*2)A	(*a* − *a*)	138	−64	(74; −140)
(*C*-*S*2)C	(*a* − *a*)	132	26	(153; −114)
(*C*-*S*2)D	(*a* − *a*)	122	−13	(101; 65)
(*C*-*S*3)A	(*a* − *ae*)	152	−80	(67; −144)
(*C*-*S*3)C	(*a* − *ae*)	149	27	(149; −103)
(*C*-*S*3)E	(*a* − *ae*)	157	161	(82; −89)
(*C*-*S*4)A	(*a* − *e*)	156	−86	(57; −161)
(*C*-*S*4)B	(*a* − *e*)	155	−11	(108; −123)
(*C*-*S*4)C	(*a* − *e*)	156	26	(140; −112)
(*C*-*S*4)E	(*a* − *e*)	165	−177	(88; 82)
(*C*-*S*5)A	(*a* − *e*)	155	−103	(43; −179)
(*C*-*S*5)B	(*a* − *e*)	156	6	(124; −131)
(*C*-*S*5)E	(*a* − *e*)	165	−177	(93; 73)
(*C*-*S*6)A	(*a* − *ae*)	153	−62	(65; −154)
(*C*-*S*6)C	(*a* − *a*)	138	49	(152; −107)
(*C*-*S*6)D	(*a* − *a*)	126	2	(82; −89)
(*C*-*S*6)E	(*a* − *e*)	149	162	(76; 59)
(*S*1-*C*)A	(*a* − *e*)	160	−63	(62; −157)
(*S*1-*C*)B	(*a* − *e*)	158	16	(130; −129)
(*S*1-*C*)E	(*a* − *e*)	162	−172	(89; 70)
(*S*2-*C*)A	(*a* − *e*)	156	−122	(36; −179)
(*S*2-*C*)B	(*a* − *e*)	155	−30	(97; −136)
(*S*2-*C*)C	(*a* − *e*)	152	30	(143; −110)
(*S*2-*C*)E	(*a* − *e*)	175	−169	(102; 82)
(*S*3-*C*)A′	(*ae* − *e*)	141	−164	(−22; −147)
(*S*3-*C*)A	(*ae* − *e*)	160	−62	(72; −133)
(*S*3-*C*)C	(*a* − *e*)	161	6	(123; −109)
(*S*3-*C*)E	(*ae* − *e*)	156	152	(84; 75)
(*S*4-*C*)A′	(*e* − *e*)	154	−172	(−39; −144)
(*S*4-*C*)A	(*e* − *e*)	170	−67	(71; −132)
(*S*4-*C*)C	(*e* − *e*)	173	15	(151; −122)
(*S*4-*C*)E	(*e* − *e*)	149	160	(89; 78)
(*S*5-*C*)A′	(*e* − *e*)	152	−167	(−34; −142)
(*S*5-*C*)A	(*e* − *e*)	168	−51	(68; −125)
(*S*5-*C*)C	(*e* − *e*)	172	38	(154; −116)
(*S*5-*C*)E	(*e* − *e*)	150	169	(84; 80)
(*S*6-*C*)A′	(*ae* − *e*)	155	−116	(13; −165)
(*S*6-*C*)B	(*a* − *e*)	160	21	(132; −127)
(*S*6-*C*)E	(*a* − *e*)	163	−166	(90; 77)

quences of the ring forms. In the $^4C_1$ chair conformation, well-identified axial and equatorial linkage types (on C_1 and C_4 atoms, respectively) can be characterized by *O*1-*C*1-*C*4 and *O*4-*C*4-*C*1 angle values. For the four low-energy conformations of the ***C*-*C*** map, these angles are about 106° and 150°. Thus, the linkage types were classified in three classes: **a** (axial), **ae** (semiaxial), and **e** (equatorial) with the following range values: **a** < 115° < **ae** < 140° < **e**.

The linkage types on C_1 and C'_4 and τ values are reported in Table V. There is a good correlation between the combination of linkage types and τ values. All low-energy conformations of ***C-C*** map are known as (**a-e**) glycosidic linkage types and give a reference value for τ ($\sim$ 157°). A very similar average value (158°) was found for all (**a-e**) types whatever the ring forms were. This curvature was less important ($\tau \sim 161°$) in the linkage type combination (**e-e**), implying that the global propagation is a little bit more linear. However, it must be mentioned that in both cases (**a-e** and **e-e**) some almost linear global propagations could be found with τ values greater than 170° (***S2-C***$_E$, ***S4-C***$_{A,C}$, and ***S5-C***$_C$). Linkage type combinations (**a-ae**) and (**ae-e**) yield more pronounced curvatures ($\tau \sim 153°$) compared to (**a-e**) combination, and this phenomenon is particularly important for (**a-a**) combination ($\tau \sim 134°$). In the later case, some very low τ values were found (124°, 122°, and 126° for ***C-S1***$_D$, ***C-S2***$_D$, and ***C-S6***$_D$, respectively), involving almost perpendicular glucopyranose rings. Table V shows that the curvatures are mainly dependent on the linkage type combinations but the location of low-energy conformations (A', A, B, **C**, D, and **E** regions) has no real influence except for D and E regions. D regions have lower τ values in comparison with corresponding linkage types, whereas the reverse phenomenon is often observed for E regions.

On the contrary, the second propagation parameter (Ω), which characterizes the relative orientation of the two mean planes, is mainly influenced by the (ϕ, φ) regions where the low-energy conformations are found. This is consistent with the fact that Ω is mainly dependent on the glycosidic linkage conformation. On the ***C-C*** map, the four low-energy conformations (located in A, B, C, and E regions) yield different and well-separated Ω values. Table V (column 2) lists all Ω values for low energy conformations. According to the classification previously defined for the low-energy regions, the average Ω values are −155°, −75°, −2°, 29°, −2°, and 174° for A', A, B, C, D, and E regions, respectively. Assuming that the extreme values found in each class correspond to lower and upper limits, Figure 8 depicts the range distribution of Ω values on superimposition to the average values. In spite of the wide range of variations, there is a very low recovery of the Ω zones, which confirms the validity of the region delimitation for this propagation parameter. The allowed variation of Ω describes an almost continuous zone representing about three-fourths of the total circle. Two couples of Ω ranges are opposite in this circular representation (A', C) and (B, E) with average values of (−144°, 26°) and (−2°, 174°), respectively. These cases correspond to a complete turnaround (π rotation) of one mean ring plane when superimposing the other one of the maltose.

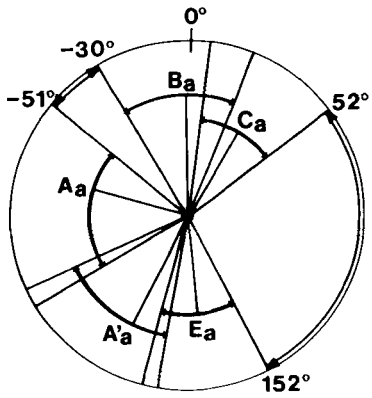

FIGURE 8 Schematic representation of the relative orientation of two mean ring planes of the maltose. A'_a, A_a, B_a, C_a, and E_a are average values of A', A, B, C, and E low-energy conformations. D conformations are not reported since D_a and range variations belongs to B domain. Filled and unfilled arcs correspond to accessible and unaccessible Ω domains, respectively.

CONCLUSIONS

The presence of a flexible conformation for one six-membered ring of the maltose molecule in an interacting context provides substantial modifications compared with well-known ***C-C*** conformations. The semirelaxed strategy used for ***C-Sx*** and ***Sx-C*** maps considerably increases the number of low-energy conformations with sets of (ϕ, φ) values significantly different from those already calculated for ***C-C*** low-energy conformations. The broader area (encompassing A', A, B, C, and D regions) has low-energy conformations well dispersed in (ϕ, φ) space and the segregation in subzones (especially for A, B, and C regions) is somewhat arbitrary. A new accessible region (A') found for ***S3-C***, ***S4-C***, ***S5-C***, and ***S6-C*** forms largely contributes to the global broadening of the accessible (ϕ, φ) zones that would be even more emphasized by a fully relaxed protocol.

More interestingly, a flexible ring form has major consequences on amylose chain propagation as analyzed by (τ, Ω) parameters. The very large variation range of τ (from 120° to 175°) allows an important curvature range apart from the glycosidic junction describing a continuous fluctuation from almost perpendicular to linear ring locations. This

result must be compared with very narrow τ variation in the ***C-C*** map and will give new insight into the local propagation of the amylose chain between adjacent subsites of catalytic enzyme regions with respect to intermediate state conformations and steric hindrance. More generally, one must keep in mind that in a flexible ring form, the linkage type could be modified both on C_1 and C_4 atoms. Therefore, the curvature modification of the amylose chain should be analyzed at each extremity of the considered flexible ring form. Finally, another important effect of flexible ring forms on the maltose is to potentially provide a very large panel of relative orientations (evaluated by Ω) between the two mean ring planes. This fact will be particularly useful for further docking analysis of the amylose chain in subsites of the amylase molecules.

REFERENCES

1. French, A. D. & Brady, J. B. (1990) in *Computer Modeling of Carbohydrates,* ACS Symposium Series 430, French, A. D. & Brady, J. B. Eds., American Chemical Society, Washington, DC, pp. 1–19.
2. Rao, V. S. R., Sundararajan, P. R., Ramakrishnan, C. & Ramachandran, G. N. (1963) in *Conformation of Biopolymers,* Vol. 2, Academic Press, London, United Kingdom.
3. Goebel, C. V., Dimpfl, W. L. & Brant, D. A. (1970) *Macromolecules* **3,** 644–654.
4. Gagnaire, D., Perez, S. & Tran, V. (1980) *Carbohydr. Res.* **78,** 849–109.
5. Brant, D. A. and Christ, M. D. (1990) "*Realistic Conformational Modeling of Carbohydrates*", ACS Symposium Series 430, French, A. D. & Brady, J. B., Eds., American Chemical Society, Washington, DC, pp. 42–68.
6. Nakata, Y., Kitamura, S., Takeo, K. & Norisuye, T. (1994) *Polymer J.* **26,** 1085–1089.
7. Rees, D. A. & Smith, P. J. (1975) *J. Chem. Soc, Perkin Trans. 2,* 836–840.
8. Perez, S., Roux, M., Revol, J. F. & Marchessault, R. H. (1979) *J. Mol. Biol.* **129,** 113–133.
9. Perez, S. & Vergelati, C. (1987) *Polym. Bull.* **17,** 141–148.
10. Ha, S. N., Madsen, L. J. & Brady, J. W. (1988) *Biopolymers* **27,** 1927–1952.
11. Tran, V., Buléon, A., Imberty, A. & Perez, S. (1989) *Biopolymers* **28,** 679–69.
12. Dowd, M. K., Zeng, J., French, A. D. & Reilly, P. J. (1992) *Carbohydr. Res.* **230,** 223–244.
13. French, A. D., Rowland, R. S. & Allinger, N. L. (1990) *Modeling of Glucopyranose,* ACS Symposium Series 430, French, A. D. & Brady, J. B., Eds., American Chemical Society, Washington, DC, pp. 120–140.
14. Sheldrick, B. & Akrigg, D. (1980) *Acta Crystallogr. Sect. B* **B36,** 1615–1621.
15. Gagnaire, D., Perez, S. & Tran, V. (1980) *Carbohydr. Res.* **82,** 185–194.
16. Thoma, J. A. & Koshland, D. E. Jr. (1960) *J. Biol. Chem.* **235,** 2511–2517.
17. Truscheit, E., Frommer, W., Junge, B., Müller, L., Schmidt, D. D. & Wingender, W. (1981) *Angew. Chem. Int. Ed. Engl.* **20,** 744–761.
18. Aleshin, A. E., Firsov, L. M. & Honzatko, R. B. (1994) *J. Biol. Chem.* **269,** 15631–15639.
19. Sigurskjold, B. W., Berland, C. R. & Svensson, B. (1994) *Biochemistry* **33,** 10191–10199 (1994).
20. Bock, K. & Pedersen, H. (1984) *Carbohydr. Res.* **132,** 142–149.
21. Stoffer, B., Aleshin, A. E., Firsov, L. M., Svensson, B. & Honzatko, R. B. (1995) *FEBS Lett.* **358,** 57–61.
22. Harris, E. M. S., Aleshin, A. E., Firsov, L. M. & Honzatko, R. B. (1993) *Biochemistry* **32,** 1618–1626.
23. Raimbaud, E., Buleon, A. & Perez, S. (1992) *Carbohydr. Res.* **227,** 351–363.
24. Takase, K. (1992) *Biochim. Biophys. Acta* **1122,** 278–282.
25. Vallée, F., Kadziola, A., Bourne, Y., Abe, J. I., Svensson, B. & Haser, R. (1994) *J. Mol. Biol.* **236,** 368–371.
26. Kadziola, A., Abe, J. I., Svensson, B. & Haser, R. (1994) *J. Mol. Biol.* **239,** 104–121.
27. Quian, M., Haser, R., Buisson, G., Duée, E. & Payan, F. (1994) *Biochemistry* **33,** 6284–6294.
28. Casset, F., Imberty, A., Haser, R., Payan, F. & Perez, S. (1995) *Eur. J. Biochem.* **232,** 284–293.
29. Kadziola, A., Søgaard, M., Svensson, B. & Haser, R., to appear.
30. Jeffrey, G. A. & Yates, J. H. (1979) *Carbohydr. Res.* **74,** 418–420.
31. Hazebroek, P. & Oosterhoff, J. (1951) *Discuss. Faraday Soc.* **10,** 87.
32. Kilpatrick, J. E., Pitzer, K. S. & Pitzer, R. (1947) *J. Am. Chem. Soc.* **69,** 2483.
33. Cremer, D. & Pople, J. A. (1947) *J. Am. Chem. Soc.* **97,** 1354–1358.
34. Dauber-Osguthorpe, P., Roberts, V. A., Osguthorpe, P. J., Wolff, J., Genest, M. & Hagler, A. T. (1988) *Proteins: Struct., Funct., Genet.* **4,** 31.
35. Godet, M. C., Tran, V., Delage, M. M. & Buléon, A. (1993) *Int. J. Biol. Macromol.* **15,** 11–15.